J. Plasma Phys. (2025), *vol*. 91, E22
Published by Cambridge University Press

doi:10.1017/S0022377824001053

Symplectic particle-in-cell methods for hybrid plasma models with Boltzmann electrons and space-charge effects

Yingzhe Li †

Max Planck Institute for Plasma Physics, Boltzmannstrasse 2, 85748 Garching, Germany

(Received 14 July 2023; revised 5 July 2024; accepted 12 July 2024)

We study the geometric particle-in-cell methods for an electrostatic hybrid plasma model. In this model, ions are described by the fully kinetic equations, electron density is determined by the Boltzmann relation and space-charge effects are incorporated through the Poisson equation. By discretizing the action integral or the Poisson bracket of the hybrid model, we obtain a finite dimensional Hamiltonian system, for which the Hamiltonian splitting methods or the discrete gradient methods can be used to preserve the geometric structure or energy. The global neutrality condition is conserved under suitable boundary conditions. Moreover, the results are further developed for an electromagnetic hybrid model proposed by Vu (*J. Comput. Phys.*, vol. 124, issue 2, 1996, pp. 417–430). Numerical experiments of finite grid instability, Landau damping and resonantly excited nonlinear ion waves illustrate the behaviour of the numerical methods constructed.

Keywords: hybrid plasma simulations, laser plasma interaction, space-charge effects, symplectic methods

1. Introduction

Hybrid plasma models with Boltzmann electrons and space-charge effects (Vu 1996; Cartwright, Verboncoeur & Birdsall 2000; Tajima 2018) constitute an important class of plasma models. In these models, the electron density is directly determined from the potential via the Boltzmann relation, and space-charge effects are included via the Poisson equation. The electrostatic hybrid model with Boltzmann electrons and space-charge effects (HBS model) has many applications in plasma physics. The acceleration of light and heavy ions in an expanding plasma slab with hot electrons produced by an intense and short laser pulse is studied using the HBS model by Bychenkov *et al.* (2004). Hu & Wang (2018), by numerical simulations of the HBS model, investigate the expansion of a collisionless hypersonic plasma plume into a vacuum. Cohen *et al.* (1997) numerically simulates resonantly excited nonlinear ion waves using the HBS model and it is noted that the exponential term in the Poisson equation introduces sufficient nonlinearity, allowing us to derive the dispersion relation for parametric instabilities and describe the generation of

† Email address for correspondence: yingzhe.li@ipp.mpg.de

the second harmonic. Mathematically, a related model with Boltzmann electrons is derived and proved to be well-posed globally by Bardos *et al.* (2018). To include electromagnetic effects, an electromagnetic hybrid model with the self-consistent ponderomotive driving potential is proposed by Vu (1996), and a more general fully kinetic, reduced-description particle-in-cell model is presented by Vu, Bezzerides & DuBois (1999) for the ion-driven parametric instabilities.

Different from the fully kinetic (for both ions and electrons) Vlasov–Poisson system, there is no electron distribution function in the HBS model. The simulations using the HBS model allow time step sizes on the scale of ions and are thus more efficient. By taking the quasi-neutral limit of the HBS model, a simplified hybrid model without the space-charge effects (Rambo 1995) can be derived. However, the space-charge effects are important and need to be incorporated in some cases (Vu 1996), such as in the inertial confined fusion regime where $k\lambda_e = \mathcal{O}(1)$, with λ_e the electron Debye length and k the wavenumber. To achieve accurate resolution at the electron Debye scale, for example, to recover numerically the $k^2\lambda_e^2$ term in the dispersion relation of the ion acoustic waves, the mesh size Δx must satisfy $\Delta x < \lambda_e$.

There have been numerous numerical methods developed for electrostatic plasma models, such as Eulerian methods (Heath *et al.* 2012; Manzini *et al.* 2016), particle-in-cell methods (Birdsall & Langdon 2018; Hockney & Eastwood 2021) and semi-Lagrangian methods (Cheng & Knorr 1976; Sonnendrücker *et al.* 1999). Recently, some structure-preserving methods have been proposed by Webb (2016) and Gu, He & Sun (2022) for the fully kinetic Vlasov–Poisson system. Structure-preserving methods for the hybrid model with quasi-neutrality and Boltzmann electrons have been developed based on variational or Hamiltonian formulations (Xiao & Qin 2019*a*; Li *et al.* 2024*a*,*b*). The nonlinear Poisson–Boltzmann equation in the HBS model appears in many electrostatic models in biomolecular simulations. For a review about fast analytical methods, see Xu & Cai (2011), and for numerical methods, see Lu *et al.* (2008). Many numerical methods have been proposed for the Poisson–Boltzmann equation, such as the finite element method (Chen, Holst & Xu 2007) and the iterative discontinuous Galerkin method (Yin, Huang & Liu 2014, 2018).

In this work, our discretizations of the HBS model follow the structure-preserving methods for models in plasma physics (Qin *et al.* 2015*b*; Xiao *et al.* 2015; He *et al.* 2016; Kraus *et al.* 2017; Morrison 2017), which preserve the geometric structures of the systems and exhibit very good long-term behaviour (Hairer, Lubich & Wanner 2006; Feng & Qin 2010). The numerical schemes constructed in this work complement existing structure-preserving methods for other (hybrid) electrostatic models. Moreover, a more complicated electromagnetic hybrid model proposed by Vu (1996) is investigated.

The action integral and Hamiltonian structure of the HBS model in this work are derived based on the results of Low (1958), Morrison (1980) and Xiao & Qin (2019*a*). By discretizing the action integral, as done by Xiao *et al.* (2015) and Xiao & Qin (2019*a*), or the Poisson bracket, as done by Qin *et al.* (2015*b*) and Kraus *et al.* (2017) with particle methods for the distribution function and finite difference methods for the electrostatic potential, we obtain a finite dimensional Hamiltonian system. Time discretizations are conducted using the Hamiltonian splitting methods (Hairer *et al.* 2006) and the discrete gradient methods (Gonzalez 1996; McLachlan, Quispel & Robidoux 1999). In plasma physics simulations, Hamiltonian splitting methods have been used by Crouseilles, Einkemmer & Faou (2015), Qin *et al.* (2015*a*), He *et al.* (2015) and discrete gradient methods have been used by Kormann & Sonnendrücker (2021) as time integrators. For the electromagnetic hybrid model (Vu 1996), a Poisson bracket is proposed

https://doi.org/10.1017/S0022377824001053 Published online by Cambridge University Press

as the sum of the Lie–Poisson bracket (Morrison 1980) and the canonical bracket of the Schrödinger equation (Marsden & Ratiu 2013).

The neutrality condition is preserved by the discretizations of the HBS model with appropriate boundary conditions. Moreover, we demonstrate that the quasi-neutral limits of the schemes proposed are structure preserving for the hybrid model with quasi-neutrality and Boltzmann electrons. The numerical methods are validated by the good conservation of energy. We conduct the implementation in the Python package STRUPHY (Holderied, Possanner & Wang 2021).

The paper is organized as follows. In § 2, the action integral and the Poisson bracket are presented for the HBS model. In § 3, structure-preserving discretizations are given. In § 4, two asymptotic limits and the dispersion relation of the linear Landau damping of the HBS model are discussed. Geometric structure and discretization of the electromagnetic hybrid model proposed by Vu (1996) are presented in § 5. In § 6, numerical experiments of finite grid instability, Landau damping and resonantly excited nonlinear ion waves are conducted to validate the numerical schemes of the HBS model. In § 7, we conclude the paper with a summary and an outlook for future works.

2. The electrostatic hybrid plasma model with Boltzmann electrons and space-charge effects

In this section, we introduce the action integral and the Poisson bracket for the HBS model (Tajima 2018), and formulate the model as a Hamiltonian system (Hairer *et al.* 2006). The electromagnetic hybrid model proposed by Vu (1996) is presented in § 5. The HBS model with physical units is

$$\left.\begin{aligned} \frac{\partial f}{\partial t} + \boldsymbol{v}\cdot\nabla f + \frac{Ze}{m_i}\boldsymbol{E}\cdot\nabla_v f = 0, \\ \boldsymbol{E} = -\nabla\phi, \\ -\epsilon_0\Delta\phi = Ze\int f\,\mathrm{d}\boldsymbol{v} - en_0\exp\left(\frac{e(\phi-\phi_0)}{k_B T_e}\right), \quad \text{Poisson–Boltzmann.} \end{aligned}\right\} \tag{2.1}$$

Here, $f(t,\boldsymbol{x},\boldsymbol{v})$ represents the distribution function of ions, which depends on time t, position $\boldsymbol{x}$ and velocity $\boldsymbol{v}$. The symbol e denotes the unit charge, m_i denotes the ion mass and Z denotes the ion charge number. The electrostatic potential $\phi(t,\boldsymbol{x})$ is determined by the Poisson–Boltzmann equation and electron density n_e is related to ϕ through the Boltzmann relation,

$$n_e = n_0\exp((\phi-\phi_0)/T_e), \quad \text{Boltzmann relation}, \tag{2.2}$$

where $n_0(t,\boldsymbol{x})$ is the reference electron number density, $\phi_0(t,\boldsymbol{x})$ is the reference potential or the low-frequency ponderomotive potential and $T_e(t,\boldsymbol{x})$ is the given temperature of electrons.

The normalization is done as

$$\begin{aligned} &\tilde{\boldsymbol{x}} = \frac{\boldsymbol{x}}{\lambda_D}, \quad \tilde{\boldsymbol{v}} = \frac{\boldsymbol{v}}{C_0}, \quad \tilde{t} = t\omega_i, \quad \tilde{f} = \frac{C_0^3}{\bar{n}}f, \\ &\tilde{n}_0 = \frac{n_0}{\bar{n}}, \quad \tilde{T}_e = \frac{T_e}{\bar{T}_i}, \quad \tilde{\phi} = \frac{e\phi}{k_B\bar{T}_i}, \quad \tilde{\phi}_0 = \frac{e\phi_0}{k_B\bar{T}_i}, \end{aligned} \tag{2.3a–h}$$

where $C_0 = \sqrt{k_B\bar{T}_i/m_i}$ is the ion thermal speed, $Z\omega_i = \sqrt{\bar{n}Z^2e^2/\epsilon_0 m_i}$ is the ion plasma frequency, $\lambda_D = C_0/\omega_i = \sqrt{\epsilon_0 k_B\bar{T}_i/\bar{n}e^2}$, $\bar{n}$ is the characteristic ion density and $\bar{T}_i$ is the

https://doi.org/10.1017/S0022377824001053 Published online by Cambridge University Press

characteristic ion temperature. Then, we get the normalized HBS model (tilde symbol is omitted for convenience)

$$\left.\begin{aligned} \frac{\partial f}{\partial t} + \boldsymbol{v}\cdot\nabla f + Z\boldsymbol{E}\cdot\nabla_v f = 0, \\ \boldsymbol{E} = -\nabla\phi, \\ -\Delta\phi = Z\int f\,\mathrm{d}\boldsymbol{v} - n_0\exp((\phi-\phi_0)/T_e), \quad \text{Poisson}-\text{Boltzmann}. \end{aligned}\right\} \tag{2.4}$$

When a periodic or zero Neumann boundary condition is imposed, the HBS model satisfies a neutrality condition given by

$$Z\int f\,\mathrm{d}\boldsymbol{x}\,\mathrm{d}\boldsymbol{v} = \int n_0\exp((\phi-\phi_0)/T_e)\,\mathrm{d}\boldsymbol{x}. \tag{2.5}$$

To construct structure-preserving methods for this model, the following action integral and Poisson bracket are proposed. For convenience, we consider the case with time independent n_0, ϕ_0, T_e. The time dependent case can be addressed using the technique of extending the dimension (Zhou *et al.* 2017).

Variational principle. By adding the term $\frac{1}{2}|\nabla\phi|^2$ in Low's action principle (Low 1958) and combining it with the action principle proposed by Xiao & Qin (2019*a*), we derive the following action integral:

$$\begin{aligned} \mathcal{A}(\boldsymbol{x},\phi) = &\int f_0(\boldsymbol{x}_0,\boldsymbol{v}_0)\left(\frac{|\dot{\boldsymbol{x}}|^2}{2} - Z\phi(\boldsymbol{x})\right)\mathrm{d}\boldsymbol{z}_0 + \int\frac{|\nabla\phi|^2}{2}\,\mathrm{d}\boldsymbol{x} \\ &+ \int n_0 T_e\exp\left(\frac{\phi-\phi_0}{T_e}\right)\mathrm{d}\boldsymbol{x}, \end{aligned} \tag{2.6}$$

where $\mathrm{d}\boldsymbol{z}_0 := \mathrm{d}\boldsymbol{x}_0\,\mathrm{d}\boldsymbol{v}_0$, $\boldsymbol{x} = \boldsymbol{x}(\boldsymbol{x}_0,\boldsymbol{v}_0,t)$, and $\dot{\boldsymbol{x}} = \mathrm{d}\boldsymbol{x}(\boldsymbol{x}_0,\boldsymbol{v}_0,t)/\mathrm{d}t$. We introduce $\boldsymbol{v} = \dot{\boldsymbol{x}}$ and $f(t,\boldsymbol{x},\boldsymbol{v}) = f_0(\boldsymbol{x}_0,\boldsymbol{v}_0)$, and the Euler–Lagrangian equations $\delta\mathcal{A}/\delta\boldsymbol{x} = 0$, $\delta\mathcal{A}/\delta\phi = 0$ can be written as

$$\ddot{\boldsymbol{x}} = -Z\nabla\phi(\boldsymbol{x}), \quad -\Delta\phi = Z\int f(t,\boldsymbol{x},\boldsymbol{v})\,\mathrm{d}\boldsymbol{v} - n_0\exp((\phi-\phi_0)/T_e), \tag{2.7}$$

which yields the HBS model (2.4) by calculating $\mathrm{d}f/\mathrm{d}t = 0$.

Poisson bracket. The Poisson bracket of this model is the same as the Vlasov–Poisson system's Poisson bracket proposed by Morrison (1980),

$$\{\mathcal{F},\mathcal{G}\}(f) = \int f\left[\frac{\delta\mathcal{F}}{\delta f},\frac{\delta\mathcal{G}}{\delta f}\right]_{xv}\mathrm{d}\boldsymbol{x}\,\mathrm{d}\boldsymbol{v}, \tag{2.8}$$

where $[g,h]_{xv} = \nabla_{\boldsymbol{x}}g\cdot\nabla_{\boldsymbol{v}}h - \nabla_{\boldsymbol{x}}h\cdot\nabla_{\boldsymbol{v}}g$. The Hamiltonian (total energy) of this model is

$$\begin{aligned} \mathcal{H} &= \int|\boldsymbol{v}|^2 f\,\mathrm{d}\boldsymbol{x}\,\mathrm{d}\boldsymbol{v} - \mathcal{A} \\ &= -\frac{1}{2}\int|\nabla\phi|^2\,\mathrm{d}\boldsymbol{x} + Z\int f\phi\,\mathrm{d}\boldsymbol{x}\,\mathrm{d}\boldsymbol{v} - \int T_e n_0\exp\left(\frac{\phi-\phi_0}{T_e}\right)\mathrm{d}\boldsymbol{x} + \frac{1}{2}\int|\boldsymbol{v}|^2 f\,\mathrm{d}\boldsymbol{x}\,\mathrm{d}\boldsymbol{v}. \end{aligned} \tag{2.9}$$

https://doi.org/10.1017/S0022377824001053 Published online by Cambridge University Press

Based on the bracket and Hamiltonian, the HBS model (2.4) can be formulated as

$$\dot{f} = \{f, \mathcal{H}\}. \tag{2.10}$$

Here, we regard f as the only unknown of the HBS model (2.4) and ϕ is determined by f from the Poisson–Boltzmann equation in (2.4).

3. Discretization

We use the particle-in-cell methods to discretize the distribution function f and finite difference methods to discretize the electrostatic potential ϕ. Two equivalent structure-preserving phase-space discretizations are obtained by discretizing the action integral and the Poisson bracket. The Hamiltonian splitting method and the discrete gradient method are used for time discretizations to preserve the geometric structure and energy, respectively. In the following, a^n and a^{n+1} represent the approximations of a at times $n\Delta t$ and $(n+1)\Delta t$, respectively, and $a^{n+1/2} = (a^n + a^{n+1})/2$, where Δt is the time step size.

3.1. *Discretization of f and ϕ*

Here, we focus on the one-dimensional case with a periodic boundary condition, but higher dimensional cases can be treated similarly. The distribution function f is approximated as

$$f_h(x, v, t) = \sum_{k=1}^{N_p} w_k S(x - x_k)\delta(v - v_k), \tag{3.1}$$

where N_p is the total particle number, and w_k, x_k and v_k denote the weight, position and velocity of the kth particle. Additionally, S is the shape function of the particle, typically chosen as a B-spline. We use the vector $\boldsymbol{X}$ to denote $(x_1, \ldots, x_{N_p})^\top$ and vector $\boldsymbol{V}$ to denote $(v_1, \ldots, v_{N_p})^\top$.

The electrostatic potential ϕ is discretized using the finite difference method, i.e.

$$\phi_j \approx \phi(x_j), \quad j = 1, \ldots, N, \tag{3.2}$$

with a set of uniform grids $\{x_j\}$, N is the number of grids, $(\phi_1, \ldots, \phi_N)^\top$ is denoted as $\boldsymbol{\phi}$ and $(\phi_0(x_1), \ldots, \phi_0(x_N))^\top$ is denoted as $\boldsymbol{\phi}_0$.

3.2. *Phase-space discretization*

3.2.1. *Discretization of action integral*

We approximate the variational action integral (2.6) as

$$\begin{aligned}\mathcal{A}_h(\boldsymbol{X}, \boldsymbol{\phi}) = &\sum_{k=1}^{N_p} w_k \left(\frac{1}{2}\dot{x}_k^2 - Z \sum_{j=1}^{N} \Delta x S(x_j - x_k)\phi_j \right) + \frac{1}{2}\boldsymbol{\phi}^\top \mathbf{A}\boldsymbol{\phi}\Delta x \\ &+ \sum_{j=1}^{N} \Delta x n_0(x_j) T_e(x_j) \exp\left(\frac{\phi_j - \phi_0(x_j)}{T_e(x_j)} \right),\end{aligned} \tag{3.3}$$

https://doi.org/10.1017/S0022377824001053 Published online by Cambridge University Press

where the matrix $\mathbf{A}$ of size $N \times N$ is

$$\mathbf{A} = \frac{1}{\Delta x^2}\begin{pmatrix} -2 & 1 & 0 & \cdots & 0 & 0 & 1 \\ 1 & -2 & 1 & 0 & \cdots & 0 & 0 \\ 0 & 1 & -2 & 1 & 0 & \cdots & 0 \\ \vdots & \ddots & \ddots & \ddots & \ddots & \ddots & \vdots \\ 0 & \cdots & 0 & 1 & -2 & 1 & 0 \\ 0 & \cdots & 0 & 0 & 1 & -2 & 1 \\ 1 & 0 & 0 & \cdots & 0 & 1 & -2 \end{pmatrix}. \tag{3.4}$$

By calculating the variations about x_k and $\boldsymbol{\phi}$, we have

$$\begin{aligned} &\ddot{x}_k = Z\sum_j \Delta x \partial_x S(x_j - x_k)\phi_j, \quad k = 1, \ldots, N_p, \\ &- Z\sum_{k=1}^{N_p} w_k S(x_j - x_k) + (\mathbf{A}\boldsymbol{\phi})_j + n_0(x_j)\exp\left(\frac{\phi_j - \phi_0(x_j)}{T_e(x_j)}\right) = 0, \quad j = 1, \ldots, N. \end{aligned} \tag{3.5}$$

REMARK 3.1. *The fixed point iteration method of Cohen et al. (1997) is used for solving the above discretized Poisson–Boltzmann equation, i.e. the second equation of (3.5),*

$$\mathbf{A}\boldsymbol{\phi}^{m+1} - c\boldsymbol{\phi}^{m+1} = -\boldsymbol{n}_i - c\boldsymbol{\phi}^m + \boldsymbol{n}_e^m, \tag{3.6}$$

where m is the iteration index, the linear system in iteration $m \to m+1$ is solved by the conjugate gradient method Kelley (1995), $\boldsymbol{n}_i$ is the ion density at grids and the electron density at the j-grid is

$$n_{e,j}^m = n_0(x_j)\exp\left(\frac{\phi_j^m}{T_e(x_j)}\right) \quad \textit{and} \quad c = \max\left\{\frac{1}{T_e(x_j)}\exp\left(\phi_j^m/T_e(x_j)\right),\ j = 1, \ldots, N\right\}. \tag{3.7a,b}$$

The initial value of the fixed point iteration is set as zero in § 6.

Equation (3.5) can be formulated as a Hamiltonian system by the Legendre transformation (Marsden & Ratiu 2013). In the following, we present another way to derive a finite dimensional Hamiltonian system.

3.2.2. *Discretization of Poisson bracket*

Here, we discretize the Poisson bracket (2.8) according to Qin *et al.* (2015*b*), Kraus *et al.* (2017) and obtain

$$\{F, G\}_h = \sum_{k=1}^{N_p} \frac{1}{w_k}\left(\partial_{x_k} F \partial_{v_k} G - \partial_{x_k} G \partial_{v_k} F\right). \tag{3.8}$$

The discrete Hamiltonian is

$$\begin{aligned} H = &-\frac{1}{2}\boldsymbol{\phi}^\top \mathbf{A}\boldsymbol{\phi}\Delta x + Z\sum_{j=1}^{N}\Delta x\sum_{k=1}^{N_p} w_k S(x_j - x_k)\phi_j + \frac{1}{2}\sum_{k=1}^{N_p} w_k v_k^2 \\ &- \sum_{j=1}^{N}\Delta x T_e(x_j) n_0(x_j)\exp\left(\frac{\phi_j - \phi_0(x_j)}{T_e(x_j)}\right), \end{aligned} \tag{3.9}$$

https://doi.org/10.1017/S0022377824001053 Published online by Cambridge University Press

where the $\boldsymbol{\phi}$ is determined by the particles via the second equation in (3.5). Then, we can obtain the following finite dimensional Hamiltonian system after phase-space discretization:

$$\dot{x}_k = \frac{1}{w_k}\partial_{v_k} H, \quad \dot{v}_k = -\frac{1}{w_k}\partial_{x_k} H, \quad k = 1, \ldots, N_p. \tag{3.10}$$

The following theorem shows that the discretizations of the action principle and the Poisson bracket as above are equivalent.

THEOREM 3.2. *The Hamiltonian system* (3.10) *is equivalent to* (3.5).

Proof. As we know that $\partial_{v_k} H = w_k v_k$, we have $\dot{x}_k = v_k$. To obtain (3.5), the only thing we need to prove is that $\partial_{x_k} H = -Z w_k \sum_{j=1}^{N} \Delta x \partial_x S(x_j - x_k)\phi_j$, which is obtained by calculating $\partial_{x_k} H$ with the discrete Poisson–Boltzmann equation (the second equation in (3.5)),

$$\begin{aligned}\partial_{x_k} H = &-Z w_k \sum_{j=1}^{N} \Delta x \partial_x S(x_j - x_k)\phi_j - \mathbf{A}\boldsymbol{\phi} \cdot \frac{\partial \boldsymbol{\phi}}{\partial x_k}\Delta x \\ &+ Z \sum_{j=1}^{N} \Delta x \sum_{k'=1}^{N_p} w_k S(x_j - x'_k)\frac{\partial \phi_j}{\partial x_k} - \sum_{j=1}^{N} \Delta x_j n_0(x_j) \exp\left(\frac{\phi_j - \phi_0(x_j)}{T_e(x_j)}\right) \cdot \frac{\partial \phi_j}{\partial x_k},\end{aligned} \tag{3.11}$$

□

where the sum of the last three terms is zero because of the discrete Poisson–Boltzmann equation (the second equation in (3.5)).

THEOREM 3.3. *The discrete neutrality is conserved by the discretizations* (3.5) *and* (3.10).

Proof. Taking the sum over j in the discrete Poisson–Boltzmann equation (the second equation in (3.5)) gives

$$-Z \sum_{j=1}^{N} \sum_{k=1}^{N_p} w_k S(x_j - x_k)\Delta x + \sum_{j=1}^{N} n_0(x_j) \exp\left(\frac{\phi_j - \phi_0(x_j)}{T_e(x_j)}\right)\Delta x = 0, \tag{3.12}$$

where we use that $\sum_j (\mathbf{A}\boldsymbol{\phi})_j = 0$. This proves the discrete neutrality. □

3.3. *Time discretization*

In this subsection, we introduce the time discretizations for (3.5) and (3.10). The first method is the Hamiltonian splitting method (Hairer *et al.* 2006), which is explicit and symplectic for (3.5) and (3.10). This method was applied by Crouseilles *et al.* (2015), Qin *et al.* (2015*a*) and He *et al.* (2015) for the Vlasov–Maxwell equations, and was used by Xiao *et al.* (2015), He *et al.* (2016) and Kraus *et al.* (2017) for the construction of the fully discrete structure-preserving methods. The other time discretization is the implicit discrete gradient method (McLachlan *et al.* 1999), which preserves the energy exactly.

https://doi.org/10.1017/S0022377824001053 Published online by Cambridge University Press

Hamiltonian splitting method. We split the Hamiltonian (3.9) as $H = H_1 + H_2$, where

$$\left.\begin{aligned} H_1 &= \frac{1}{2}\sum_{k=1}^{N_p} w_k v_k^2, \\ H_2 &= -\frac{1}{2}\boldsymbol{\phi}^\top \mathbf{A}\boldsymbol{\phi}\Delta x + Z\sum_{j=1}^{N}\Delta x\sum_{k=1}^{N_p} w_k S(x_j - x_k)\phi_j \\ &\quad - \sum_{j=1}^{N}\Delta x T_e(x_j) n_0(x_j)\exp\left(\frac{\phi_j - \phi_0(x_j)}{T_e(x_j)}\right), \end{aligned}\right\} \tag{3.13}$$

which give the following two corresponding subsystems,

$$\left.\begin{aligned} &\text{sub-step I}: \dot{x}_k = v_k, \quad \dot{v}_k = 0, \\ &\text{sub-step II}: \dot{x}_k = 0, \quad \dot{v}_k = Z\sum_{j=1}^{N}\Delta x \partial_x S(x_j - x_k)\phi_j, \end{aligned}\right\} \tag{3.14}$$

where $\phi_j (j = 1, \ldots, N)$ are given by the discrete Poisson–Boltzmann equation (the second equation in (3.5)). Both sub-steps can be solved exactly. Here, we present the first- and second-order methods by the composition method (Hairer *et al.* 2006),

$$\left.\begin{aligned} &\text{First-order Lie splitting}: \Phi^1_{\Delta t}\circ\Phi^2_{\Delta t}, \\ &\text{Second-order Strang splitting}: \Phi^2_{\Delta t/2}\circ\Phi^1_{\Delta t}\circ\Phi^2_{\Delta t/2}, \end{aligned}\right\} \tag{3.15}$$

where $\Phi^1_{\Delta t}$ and $\Phi^2_{\Delta t}$ are solution maps of sub-steps I and II, respectively. Higher order structure-preserving schemes can be constructed by composition methods (Hairer *et al.* 2006).

Discrete gradient method. We use the second-order discrete gradient method proposed by Gonzalez (1996) to conserve energy exactly,

$$\frac{\boldsymbol{X}^{n+1} - \boldsymbol{X}^n}{\Delta t} = \mathbf{W}^{-1}\bar{\nabla}_{\boldsymbol{V}} H, \quad \frac{\boldsymbol{V}^{n+1} - \boldsymbol{V}^n}{\Delta t} = -\mathbf{W}^{-1}\bar{\nabla}_{\boldsymbol{X}} H, \tag{3.16a,b}$$

where

$$\left.\begin{aligned} \mathbf{W} &= \mathrm{diag}(w_1, \ldots, w_{N_p}), \\ \bar{\nabla}_{\boldsymbol{X}} H &= \nabla_{\boldsymbol{X}} H\left(\frac{\boldsymbol{X}^n + \boldsymbol{X}^{n+1}}{2}\right) + d_c\left(\boldsymbol{X}^{n+1} - \boldsymbol{X}^n\right), \\ \bar{\nabla}_{\boldsymbol{V}} H &= \nabla_{\boldsymbol{V}} H\left(\frac{\boldsymbol{V}^n + \boldsymbol{V}^{n+1}}{2}\right) + d_c\left(\boldsymbol{V}^{n+1} - \boldsymbol{V}^n\right), \\ d_c &= \frac{H_d - \nabla H(\boldsymbol{X}^{n+1/2}, \boldsymbol{V}^{n+1/2})\cdot((\boldsymbol{X}^{n+1} - \boldsymbol{X}^n)^\top, (\boldsymbol{V}^{n+1} - \boldsymbol{V}^n)^\top)^\top}{|\boldsymbol{X}^{n+1} - \boldsymbol{X}^n|^2 + |\boldsymbol{V}^{n+1} - \boldsymbol{V}^n|^2}, \\ H_d &= H(\boldsymbol{H}^{n+1}, \boldsymbol{V}^{n+1}) - H(\boldsymbol{X}^n, \boldsymbol{V}^n). \end{aligned}\right\} \tag{3.17}$$

This discrete gradient method is implicit, for which the fixed-point iteration method is used. The degree of shape function S is chosen to be at least two for the convergence of iterations.

https://doi.org/10.1017/S0022377824001053 Published online by Cambridge University Press

4. Asymptotic limits

In this section, we discuss two asymptotic limits, quasi-neutral limit and large T_e limit, with corresponding suitable normalization.

4.1. *Quasi-neutral limit*

We do the normalization as

$$\tilde{\boldsymbol{x}} = \frac{\boldsymbol{x}}{x^*}, \quad \tilde{\boldsymbol{v}} = \frac{\boldsymbol{v}}{C_0}, \quad \tilde{t} = t\omega_i, \quad \tilde{f} = \frac{C_0^3}{\bar{n}} f,$$
$$\tilde{n}_0 = \frac{n_0}{\bar{n}}, \quad \tilde{\phi} = \frac{e\phi}{k_B \bar{T}_e}, \quad \tilde{\phi}_0 = \frac{e\phi_0}{k_B \bar{T}_e}, \quad \tilde{T}_e = \frac{T_e}{\bar{T}_e}, \tag{4.1a–h}$$

where x^* is the space scale of interest, $Z\omega_i = \sqrt{\bar{n}Z^2e^2/\epsilon_0 m_i}$ is the ion plasma frequency, $\lambda_D = \sqrt{\epsilon_0 k_B \bar{T}_e/\bar{n}e^2}$ is the electron Debye length, $C_0 = \lambda_D\omega_i = \sqrt{k_B\bar{T}_e/m_i}$, $\bar{n}$ is the characteristic ion density and $\bar{T}_e$ is the characteristic electron temperature. Then, we get the normalized HBS model (tilde symbol is omitted for convenience)

$$\left.\begin{aligned} \frac{\partial f}{\partial t} + \boldsymbol{v}\cdot\nabla f + Z\boldsymbol{E}\cdot\nabla_v f = 0, \\ \boldsymbol{E} = -\nabla\phi, \\ -\lambda^2\Delta\phi = Z\int f\,\mathrm{d}\boldsymbol{v} - n_0\exp\left(\frac{\phi-\phi_0}{T_e}\right), \quad \text{Poisson–Boltzmann}, \end{aligned}\right\} \tag{4.2}$$

where $\lambda = \lambda_D/x^*$.

When we take the quasi-neutral limit $\lambda \to 0$ for the normalized HBS model (4.2), we get the following hybrid model with quasi-neutrality and Boltzmann electrons (Rambo 1995; Xiao & Qin 2019*a*):

$$\left.\begin{aligned} \frac{\partial f}{\partial t} + \boldsymbol{v}\cdot\nabla f + Z\boldsymbol{E}\cdot\nabla_v f = 0, \\ \boldsymbol{E} = -\nabla\phi, \\ 0 = Z\int f\,\mathrm{d}\boldsymbol{v} - n_0\exp\left(\frac{\phi-\phi_0}{T_e}\right). \end{aligned}\right\} \tag{4.3}$$

By the similar calculations for the Vlasov–Poisson equation as Sonnendrücker (2017), we get the dispersion relation of the linear Landau damping of (4.2) with $Z = 1$, $n_0 = 1$, $\phi_0 = 0$,

$$1 + \lambda^2 k^2 T_e = \frac{T_e}{T_i}\mathcal{Z}'\left(\frac{\omega}{kv_T}\right), \tag{4.4}$$

where $\mathcal{Z}$ is the plasma dispersion function and $T_i = v_T^2/2$. By $\lambda \to 0$, we get the dispersion relation of (4.3) (Kunz, Stone & Bai 2014),

$$1 = \frac{T_e}{T_i}\mathcal{Z}'\left(\frac{\omega}{kv_T}\right). \tag{4.5}$$

https://doi.org/10.1017/S0022377824001053 Published online by Cambridge University Press

Under this normalization (4.1*a–h*), the discrete Poisson–Boltzmann equation in our scheme (3.14) becomes

$$-Z\sum_{k=1}^{N_p} w_k S(x_j - x_k) + \lambda^2(\mathbf{A}\boldsymbol{\phi})_j + n_0(x_j)\exp\left(\frac{\phi_j - \phi_0(x_j)}{T_e(x_j)}\right) = 0, \quad j = 1, \ldots, N. \tag{4.6}$$

When taking the quasi-neutral limit for the scheme (3.14) with (4.6), we get the following structure-preserving scheme similar to the scheme proposed by Xiao & Qin (2019*a*) derived using discrete exterior calculus and Whitney form,

$$\left.\begin{aligned} &\text{sub-step I}: \dot{x}_k = v_k, \quad \dot{v}_k = 0, \\ &\text{sub-step II}: \dot{x}_k = 0, \quad \dot{v}_k = Z\sum_{j=1}^{N} \Delta x \partial_x S(x_j - x_k)\phi_j, \end{aligned}\right\} \tag{4.7}$$

where $\phi_j, j = 1, \ldots, N$ are determined by the following discrete equation about $\boldsymbol{\phi}$,

$$-Z\sum_{k=1}^{N_p} w_k S(x_j - x_k) + n_0(x_j)\exp\left(\frac{\phi_j - \phi_0(x_j)}{T_e}\right) = 0, \quad j = 1, \ldots, N. \tag{4.8}$$

Then the limiting scheme (4.7) is the Hamiltonian splitting method for the quasi-neutral limit model (4.3), i.e. scheme (3.14), and is asymptotic preserving (Jin 1999) and structure-preserving at the same time. Similarly, the discrete gradient method (3.16*a*,*b*) for the HBS model becomes a discrete gradient method for the hybrid model with quasi-neutrality and Boltzmann electrons. Note that quasi-neutral limit is not a singular asymptotic limit as explained by Degond *et al.* (2012) for the case of the Euler–Poisson–Boltzmann model.

4.2. *Large T_e limit*

Here, we adopt the normalization (2.3*a–h*). By taking the $T_e \to +\infty$ in (2.4), we get the equations

$$\left.\begin{aligned} \frac{\partial f}{\partial t} + \boldsymbol{v}\cdot\nabla f + Z\boldsymbol{E}\cdot\nabla_v f = 0, \\ \boldsymbol{E} = -\nabla\phi, \\ -\Delta\phi = Z\int f\,\mathrm{d}\boldsymbol{v} - n_0. \end{aligned}\right\} \tag{4.9}$$

Dividing by k^2T_e on both sides of the dispersion relation (4.4) of (2.4), we get the the following dispersion relation with the current normalization:

$$1 + \frac{1}{k^2T_e} = \frac{1}{k^2T_i}\mathcal{Z}'\left(\frac{\omega}{kv_T}\right). \tag{4.10}$$

By $T_e \to +\infty$, we get the dispersion relation of model (4.9) (Sonnendrücker 2017),

$$1 = \frac{1}{k^2T_i}\mathcal{Z}'\left(\frac{\omega}{kv_T}\right). \tag{4.11}$$

Similar to the quasi-neutral limit, when $T_e \to +\infty$, the limiting schemes of the Hamiltonian splitting method (3.14) and the discrete gradient method (3.16*a*,*b*) become the Hamiltonian splitting method and the discrete gradient method for model (4.9).

https://doi.org/10.1017/S0022377824001053 Published online by Cambridge University Press

5. Electromagnetic hybrid model

Here, we extend the aforementioned structure-preserving methods to an electromagnetic hybrid model with Boltzmann electrons and space charge effects proposed by Vu (1996). This model is derived using a temporal WKB approximation when there is a laser with high frequency w_0 injected into the plasma, such that numerical simulations on the time scale of the ions can be conducted. We assume the vector potential can be written as

$$\frac{1}{2}\left(\boldsymbol{a}(\boldsymbol{x},t)\mathrm{e}^{-\mathrm{i}w_0 t}+\boldsymbol{a}^*(\boldsymbol{x},t)\mathrm{e}^{\mathrm{i}w_0 t}\right), \tag{5.1}$$

where $\boldsymbol{a}=(a_1,a_2,a_3)^\top=\boldsymbol{a}_r+\mathrm{i}\boldsymbol{a}_i$ is complex-valued and is assumed to vary on a time scale much longer than $2\pi/w_0$, and $*$ denotes the conjugate of the complex number. More details of the derivation can be found from Vu (1996). After the following normalization:

$$\frac{t}{\tilde{t}}=\omega_i^{-1},\quad \frac{\boldsymbol{x}}{\tilde{\boldsymbol{x}}}=c\omega_i^{-1},\quad \frac{\boldsymbol{v}}{\tilde{\boldsymbol{v}}}=c,\quad \frac{f}{\tilde{f}}=\frac{n_c}{c^3},\quad \frac{\boldsymbol{a}}{\tilde{\boldsymbol{a}}}=\frac{cm_i}{e},\quad \frac{\phi}{\tilde{\phi}}=\frac{c^2m_i}{e},$$
$$\frac{T_e}{\tilde{T}_e}=m_ic^2,\quad \omega_i=\sqrt{\frac{n_ce^2}{m_i\epsilon_0}}, \tag{5.2a–h}$$

where c is the speed of light and n_c is the characteristic density, we have the normalized hybrid model (Vu 1996),

$$\left.\begin{aligned}
&\frac{\partial f}{\partial t}+\boldsymbol{v}\cdot\frac{\partial f}{\partial \boldsymbol{x}}+\left(-Z\nabla\phi-\frac{Z^2}{4}\nabla(\boldsymbol{a}\cdot\boldsymbol{a}^*)\right)\cdot\frac{\partial f}{\partial \boldsymbol{v}}=0,\\
&\mathrm{i}\epsilon\frac{\partial \boldsymbol{a}}{\partial t}=-\frac{\epsilon^2}{2}\Delta\boldsymbol{a}-\frac{1}{2}\left(1-\epsilon^2Z^2\int f\,\mathrm{d}\boldsymbol{v}-\epsilon^2n_e\frac{m_i}{m_e}\right)\boldsymbol{a},\quad \omega_i^2=\frac{e^2n_c}{m_i\epsilon_0},\quad \epsilon=\frac{\omega_i}{w_0}\\
&-\Delta\phi=Z\int f\,\mathrm{d}\boldsymbol{v}-n_e,
\end{aligned}\right\} \tag{5.3}$$

where Z is the ion charge number, ϵ is very small due to high frequency w_0 of the pump wave, and n_e is determined by the potential ϕ and $\boldsymbol{a}$ via the following relations with the given functions n_0 and C:

$$n_e=n_0\exp\left(\frac{\phi-\dfrac{m_i}{4m_e}\boldsymbol{a}\cdot\boldsymbol{a}^*}{T_e}\right)\quad \text{(isothermal electron case)}, \tag{5.4}$$

$$n_e=\left(\frac{\phi-\dfrac{m_i}{4m_e}\boldsymbol{a}\cdot\boldsymbol{a}^*}{T_e}\frac{\gamma-1}{\gamma}-C\right)^{1/(\gamma-1)},\ \gamma\neq 1,\quad \text{(adiabatic electron case)}. \tag{5.5}$$

The equation satisfied by $\boldsymbol{a}$ is a Schrödinger-type equation in the form similar to the semiclassical regime (Bao, Jin & Markowich 2002). Although the small parameter ϵ in the Schrödinger equation introduces strong oscillations, the time step size larger than ϵ is used by Vu (1996). The commonly used numerical scheme for the Schrödinger equation in the semiclassical regime is the time splitting spectral method (Bao *et al.* 2002), which has

https://doi.org/10.1017/S0022377824001053 Published online by Cambridge University Press

the advantage of using large time step sizes and mesh sizes, especially for the computation about the observables, such as the term $\boldsymbol{a}\cdot\boldsymbol{a}^*$ in this hybrid model.

Regarding the geometric structure, we propose the following Poisson bracket, which is the sum of the Poisson brackets of the HBS model (2.4) and the Schrödinger equation (Marsden & Ratiu 2013) (scaled by ϵ):

$$\{\mathcal{F},\mathcal{G}\}(f,\boldsymbol{a}^r,\boldsymbol{a}^i)=\int f\left[\frac{\delta\mathcal{F}}{\delta f},\frac{\delta\mathcal{G}}{\delta f}\right]_{xv}\mathrm{d}\boldsymbol{x}\,\mathrm{d}\boldsymbol{v}+\epsilon\int\frac{\delta F}{\delta\boldsymbol{a}^r}\cdot\frac{\delta G}{\delta\boldsymbol{a}^i}-\frac{\delta F}{\delta\boldsymbol{a}^i}\cdot\frac{\delta G}{\delta\boldsymbol{a}^r}\,\mathrm{d}\boldsymbol{x}. \tag{5.6}$$

The above model (5.3) can be derived with the above Poisson bracket (5.6) and the following Hamiltonian for the isothermal and adiabatic electron cases, respectively:

$$\left.\begin{aligned}\mathcal{H}=&\int\frac{|\boldsymbol{v}|^2}{2}f\,\mathrm{d}\boldsymbol{v}\,\mathrm{d}\boldsymbol{x}+\int\frac{|Z\boldsymbol{a}|^2}{4}f\,\mathrm{d}\boldsymbol{v}\,\mathrm{d}\boldsymbol{x}+\frac{1}{4}\int|\nabla a_1|^2+|\nabla a_2|^2+|\nabla a_3|^2\,\mathrm{d}\boldsymbol{x}\\&-\int\frac{|\boldsymbol{a}|^2}{4\epsilon}\,\mathrm{d}\boldsymbol{x}-\int T_e n_0\exp\left(\frac{\phi-\dfrac{m_i}{4m_e}\boldsymbol{a}\cdot\boldsymbol{a}^*}{T_e}\right)\mathrm{d}\boldsymbol{x}-\int\frac{|\nabla\phi|^2}{2}\,\mathrm{d}\boldsymbol{x}+\int Zf\phi\,\mathrm{d}\boldsymbol{x}\,\mathrm{d}\boldsymbol{v},\\ \mathcal{H}=&\int\frac{|\boldsymbol{v}|^2}{2}f\,\mathrm{d}\boldsymbol{v}\,\mathrm{d}\boldsymbol{x}+\int\frac{|Z\boldsymbol{a}|^2}{4}f\,\mathrm{d}\boldsymbol{v}\,\mathrm{d}\boldsymbol{x}+\frac{1}{4}\int|\nabla a_1|^2+|\nabla a_2|^2+|\nabla a_3|^2\,\mathrm{d}\boldsymbol{x}-\int\frac{|\boldsymbol{a}|^2}{4\epsilon}\,\mathrm{d}\boldsymbol{x}\\&-\int T_e\left(\frac{\phi-\dfrac{m_i}{4m_e}\boldsymbol{a}\cdot\boldsymbol{a}^*}{T_e}\frac{\gamma-1}{\gamma}-C\right)^{\gamma/(\gamma-1)}\mathrm{d}\boldsymbol{x}-\int\frac{|\nabla\phi|^2}{2}\,\mathrm{d}\boldsymbol{x}+\int Zf\phi\,\mathrm{d}\boldsymbol{x}\,\mathrm{d}\boldsymbol{v}.\end{aligned}\right\} \tag{5.7}$$

The phase-space discretization can be conducted as above through the discretization of the Poisson bracket as done by Qin *et al.* (2015*b*) and Kraus *et al.* (2017) or by Fourier particle methods (Campos Pinto *et al.* 2024). The Hamiltonian splitting method (Crouseilles *et al.* 2015; Qin *et al.* 2015*a*; He *et al.* 2015) gives three explicitly solvable subsystems (or in Fourier space), further details are presented in Appendix B.

6. Numerical experiments

In this section, three numerical experiments: finite grid instability (of an equilibrium), Landau damping (of damping waves) and resonantly excited nolinear ion waves (with non-zero ϕ_0), are conducted using the normalization (2.3*a–h*) to illustrate the conservation properties of the schemes (3.14)–(3.16*a*,*b*) of the HBS model (2.4). The reference density n_0 is set to 1 and the unit charge number $Z=1$. The degree of the shape function is 2, the tolerance for the fixed point iteration is 10^{-12} and periodic boundary conditions are used.

6.1. *Finite grid instability*

Finite grid instability in the context of hybrid simulations was first reported by Rambo (1995) for the hybrid model with quasi-neutrality and Boltzmann electrons. This numerical phenomenon typically arises in standard particle-in-cell methods when the temperature ratio $T_e/T_i\gg 1$, and ions are heated until the ion thermal speed becomes comparable to the ion acoustic speed (and therefore, $T_e/T_i\approx 1$). Rambo (1997) noted that finite grid instability also occurs when using traditional particle-in-cell methods for the HBS model, although it is weaker than the hybrid model with quasi-neutrality and Boltzmann electrons. Stanier, Chacón & Chen (2019) and Li *et al.* (2024*a*,*b*) numerically reduced the finite grid instability by using the conservative or bracket-based particle-in-cell methods for the hybrid model with quasi-neutrality and massless electrons. The finite grid instability of particle-in-cell methods has also been studied by Huang *et al.* (2016)

https://doi.org/10.1017/S0022377824001053 Published online by Cambridge University Press

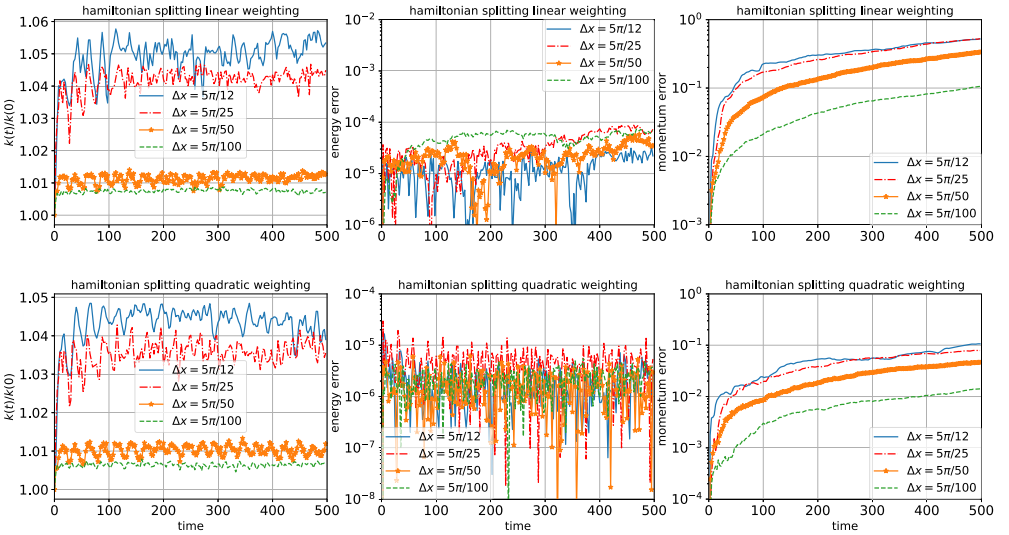

FIGURE 1. Finite grid instability of the HBS model by Hamiltonian splitting method. Time evolution of $k(t)/k(0)$ with k denoting the ion kinetic energy, relative energy error and momentum error.

and Xiao & Qin (2019*b*), which reveals that the aliased spatial modes are the major cause of the finite grid instability in the particle-in-cell methods, and geometric particle-in-cell methods are able to suppress the finite grid instability.

In this test, we investigate the finite grid instability using the following initial condition (an equilibrium of (2.4)) by the numerical simulations conducted with schemes (3.14) and (3.16*a*,*b*),

$$f = \frac{n_i}{\pi^{1/2} v_T^{1/2}} \exp\left(\frac{|v-0.1|^2}{v_T^2}\right), \quad T_e = 0.08, \quad v_T = 0.1, \quad n_i = 1. \tag{6.1}$$

Computational parameters include: domain $[0, 5\pi]$, time step size $\Delta t = 0.05$ and particle number per cell 100. We run the simulations with the numerical methods (3.14) and (3.16*a*,*b*) with different cell sizes, i.e. $\Delta x = 5\pi/12, 5\pi/25, 5\pi/50, 5\pi/100$, and the results are presented in figures 1 and 2. We can see $k(t)/k(0)$ ($k(t) = \frac{1}{2}\sum_{k=1}^{N_p} w_k v_k^2$ the ion kinetic energy) oscillates with time without exhibiting rapid linear growth, as observed in figure 3(*a*) of Rambo (1997). This indicates that the finite grid instability is reduced numerically. As the cell size decreases and the electron Debye length is resolved with higher resolution, the oscillating level of $k(t)/k(0)$ becomes closer to 1 and the momentum error also becomes smaller. The momentum error also depends on the particle number. When there are 100 cells and 2000 particles in each, the Hamiltonian splitting method with quadratic weighting gives the momentum error at the level of 10^{-4}.

As the derivatives of B-splines appear in the schemes (3.14) and (3.16*a*,*b*), second-order at least B-spline shape functions should be used. As the Hamiltonian splitting method (3.14) (Strang splitting) is symplectic, it has superior long-time numerical behaviour, although energy is not conserved exactly (with a relative error of approximately 10^{-5}) with quadratic weighting. In figure 1, the relative energy error is also very small (10^{-4}) even when the first order B-spine is used (the derivative of the B-spine is taken as its right derivative). Relative energy error of the discrete gradient method with quadratic weighting is approximately 10^{-13}.

https://doi.org/10.1017/S0022377824001053 Published online by Cambridge University Press

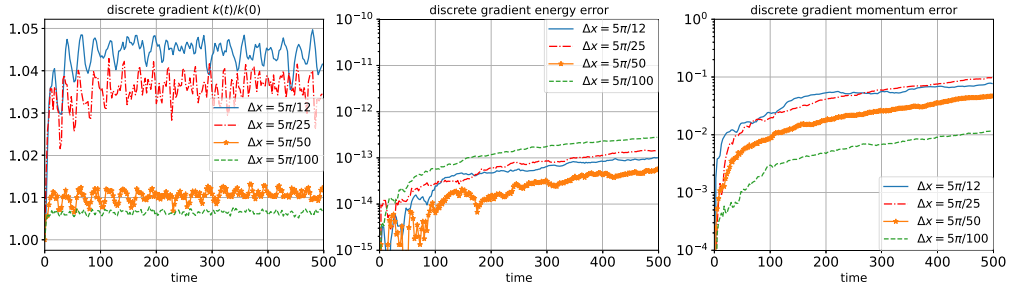

FIGURE 2. Finite grid instability of the HBS model by discrete gradient method with quadratic weighting. Time evolution of $k(t)/k(0)$ with k denoting the ion kinetic energy, relative energy error and momentum error.

Here, we discuss the time step size of the Hamiltonian splitting methods. We consider the case with 100 cells in space, time interval [0, 500] and quadratic weighting. To achieve satisfying results, when $n_i = 1$ and the number of particles per cell is 100, the maximum time step size is 0.5 approximately with energy error at the level of 10^{-4}. For higher initial densities, such as $n_i = 4, 16$ with 400, 1600 particles per cell, the maximum time step sizes giving satisfying results are approximately 0.3, 0.3 with energy errors at the level of 10^{-4}, 10^{-4}, respectively.

6.2. *Landau damping*

First, we simulate the linear ion Landau damping by one-dimensional simulations. The initial distribution function is

$$f = \frac{n_i}{\pi^{1/2} v_T^{1/2}} (1 + 0.02\cos(0.25x)) \exp\left(-\frac{v^2}{v_T^2}\right). \tag{6.2}$$

The computational parameters are as follows: grid number 64, domain size $[0, 8\pi]$, time step size $\Delta t = 0.05$, final computation time 20, $v_T = 1.4142$, $n_i = 1$ and total particle number 10^7. In this test, the quadratic weighting is used. See the numerical results with $T_e = 5$ in figure 3 by the Hamiltonian splitting method (3.14) and discrete gradient method (3.16*a*,*b*). Solving the dispersion relation mentioned in § 4, $1 + k^2 T_e = (T_e/T_i)\mathcal{Z}'(\omega/kv_T)$, we find $\omega = 0.6986 - 0.0810\mathrm{i}$ when $k = 0.25$. Methods (3.14)–(3.16*a*,*b*) give an accurate damping rate of the electric energy $\frac{1}{2}\int |\nabla\phi|^2 \,\mathrm{d}x$. The dispersion relation $1 = (T_e/T_i)\mathcal{Z}'(\omega/kv_T)$ of the model with quasi-neutrality and Boltzmann electrons (Xiao & Qin 2019*a*) in § 4 yields $\omega = 0.7528 - 0.05806\mathrm{i}$, i.e. a slower damping rate. The energy errors of the schemes (3.14)–(3.16*a*,*b*) are approximately 10^{-4} and 10^{-13}, respectively.

Then, we simulate nonlinear ion Landau damping. The initial distribution function is

$$f = \frac{n_i}{\pi^{1/2} v_T^{1/2}} (1 + 0.5\cos(0.5x)) \exp\left(-\frac{v^2}{v_T^2}\right). \tag{6.3}$$

The computational parameters are as follows: grid number 65, domain size $[0, 4\pi]$, time step size $\Delta t = 0.05$, final computation time 40, $v_T = 1.4142$, $n_i = 1$ and total particle number 10^5. In this test, the quadratic weighting is used. See the numerical results with large $T_e = 100$ in figure 4 by the Hamiltonian splitting method (3.14) and discrete gradient method (3.16*a*,*b*). Due to the large T_e, the term $\exp(\phi/T_e)$ approximates 1, making the solution of the HBS model (2.4) approximate the solution of the Vlasov–Poisson system

https://doi.org/10.1017/S0022377824001053 Published online by Cambridge University Press

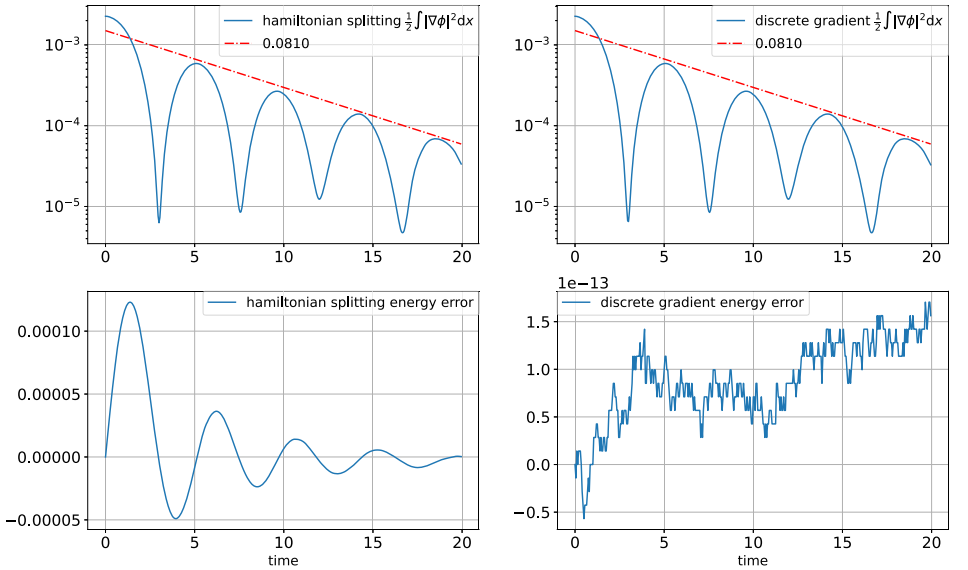

FIGURE 3. Linear Landau damping of the HBS model with $T_e = 5$ by Hamiltonian splitting and discrete gradient methods. Time evolution of the electric energy $\frac{1}{2}\int|\nabla\phi|^2\,\mathrm{d}x$ and total energy error.

(with static electron density as 1). In figure 4, we observe the nonlinear Landau damping. The time evolution of energy component $\frac{1}{2}\int|\nabla\phi|^2\,\mathrm{d}x$ decays exponentially initially, and the decay rate is very close to the decay rate 0.2854 of the Vlasov–Poisson system (Kraus *et al.* 2017) before time $T = 10$. Here, $\frac{1}{2}\int|\nabla\phi|^2\,\mathrm{d}x$ oscillates when $t \in [10, 30]$, then grows exponentially with time when $t \in [30, 40]$ with a rate close to 0.086671 (Kraus *et al.* 2017) of the Vlasov–Poisson system. For the Hamiltonian splitting method, the energy error is approximately 10^{-2}. The discrete gradient method gives a smaller total energy error of approximately 10^{-12}, and a similar behaviour of the electric energy is presented. The errors of neutrality given by both numerical methods are at the level of iteration tolerance. For the time step size of the Hamiltonian splitting methods, we consider the case with 65 cells in space, time interval $[0, 40]$, 10^5 particles and quadratic weighting. As $T_e = 100$ is large, $\exp(\phi/T_e)$ is close to 1, the numerical stability property is close to the result of Kormann & Sonnendrücker (2021), i.e. the stability condition is approximately $\Delta t\omega_i < 2$. To get the acceptable accuracy, the time step size is usually chosen smaller than 2. When $n_i = 1$, the maximum time step size yielding good numerical behaviour is $\Delta t = 0.4$, resulting in an energy error of approximately 0.45 after saturation; for $n_i = 4$, $\Delta t = 0.2$ gives an energy error of approximately 0.4 after saturation, and for $n_i = 16$, $\Delta t = 0.12$ results in an energy error of approximately 0.3 after saturation. We also consider the case with a small electron temperature $T_e = 1$. In this case, when $n_i = 1$, $\Delta t = 0.5$ gives an energy error of approximately 0.05 after saturation; when $n_i = 4$, $\Delta t = 0.2$ gives an energy error of approximately 0.002 after saturation; when $n_i = 16$, $\Delta t = 0.1$ gives an energy error of approximately 0.004.

6.3. *Simulations with the ponderomotive driving term*

Cohen *et al.* (1997) numerically solved the HBS model with a ponderomotive driving term to study nonlinear ion acoustic waves. Here, following Cohen *et al.* (1997), we conduct a simulation with a non-zero given time-dependent function ϕ_0 in (2.4). Specifically, the

https://doi.org/10.1017/S0022377824001053 Published online by Cambridge University Press

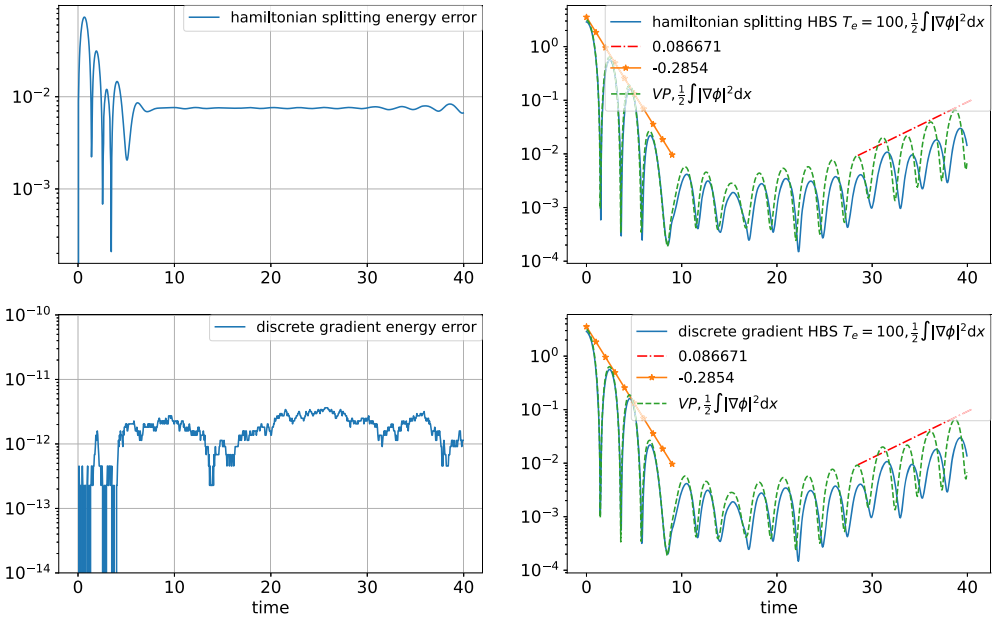

FIGURE 4. Nonlinear Landau damping of the HBS model with $T_e = 100$ by Hamiltonian splitting and discrete gradient methods. Time evolution of total energy error and electric energy $\frac{1}{2}\int|\nabla\phi|^2\,\mathrm{d}x$.

initial condition and ϕ_0 are given by

$$f = \frac{n_i}{\pi^{1/2}v_T^{1/2}}\exp\left(-\frac{v^2}{v_T^2}\right), \quad \phi_0 = \tilde{\phi}_0\cos(\Omega t - kx), \tag{6.4}$$

where $n_i = 1$, $v_T = \frac{\sqrt{2}}{10}$, $\tilde{\phi}_0 = 0.05T_e$, $\Omega = 0.4472$, $k = 1.49$. Other computational parameters are: grid number 64, domain size $[0, 10\pi/k]$, time step size $\Delta t = 0.1$, final computation time 600, $T_e = 0.1125$ and total particle number 10^6. In this test, the quadratic weighting is used. Since ϕ_0 is time dependent, the Hamiltonian system (3.10) is a non-autonomous Hamiltonian system, for which we use the the technique of extending the dimension (Zhou *et al.* 2017). From figures 5 and 6, we can see that the peak value of the response function $R(t) = \max_x(\phi/\phi_0)$ is approximately 5, which is consistent with the result of Cohen *et al.* (1997). There are a rapid oscillation at 2.1Ω and a slow modulation at 0.04Ω in the fourth figure obtained by the fast Fourier transformation of $\max_x(\phi/\phi_0)$ in time, which are close to the results of Cohen *et al.* (1997) with 1.85Ω (fast) and 0.15Ω (slow). The Hamiltonian splitting method and discrete gradient method give the energy errors of approximately 10^{-5} and 10^{-12}, respectively. Additionally, when $t = 400$, both methods give similar five vortices in phase-space contour plots, due to the driving force being the fifth mode, i.e. $k = 5(2\pi/L)$, where L is the domain size.

Regarding the time step size for the Hamiltonian splitting methods, we use the same parameters as above but vary the initial density and time step size. When the initial density $n_i = 1$, the maximum step size for giving good numerical behaviour is $\Delta t = 1.5$, which gives an energy error of approximately 0.003; When the initial density $n_i = 4$, the maximum step size $\Delta t = 1$ gives an energy error of approximately 0.02; when the initial

https://doi.org/10.1017/S0022377824001053 Published online by Cambridge University Press

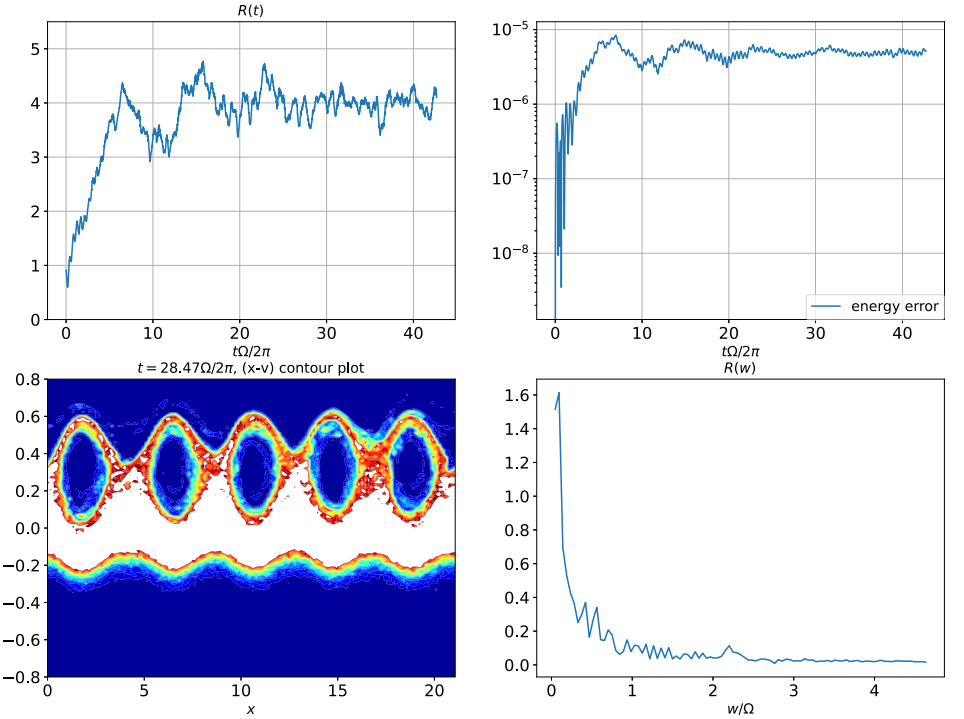

FIGURE 5. Simulations with the ponderomotive driving term by Hamiltonian splitting method. Time evolutions of $R(t) = \max(\phi/\tilde{\phi}_0)$ and energy error, the contour plot of the distribution function at time $t = 400$, and the fast Fourier transformation of $R(t)$.

density $n_i = 16$, the maximum step size $\Delta t = 0.5$ gives an energy error of approximately 0.008.

7. Conclusion

In this paper, we explore the structure-preserving discretizations of the electrostatic hybrid plasma model with Boltzmann electrons and space-charge effects. These discretizations are derived by discretizing either the variational action integral or the Poisson bracket combined with the Hamiltonian splitting methods (Crouseilles *et al.* 2015; He *et al.* 2015; Qin *et al.* 2015*a*) in time. Discrete gradient methods (McLachlan *et al.* 1999) are employed to conserve energy exactly. The geometric structure and numerical discretization of the electromagnetic hybrid model (Vu 1996) are detailed in § 5.

For discretizing the field functions, the finite element methods (Kraus *et al.* 2017) or Fourier spectral methods (Campos Pinto *et al.* 2024) can be used, while the distribution function can be discretized by the delta functions. Additional details can be found in Appendix A. The cases with other kinds of boundary conditions and further exploration (such as the physical application and the time and mesh size strategy) of the electromagnetic hybrid model can be considered in future works.

Acknowledgements

The simulations in this work were performed at the Max Planck Computing & Data Facility (MPCDF). The author would like to thank the anonymous reviewers for many helpful comments for improving this paper. Special thanks to B.I. Cohen for the help of the

https://doi.org/10.1017/S0022377824001053 Published online by Cambridge University Press

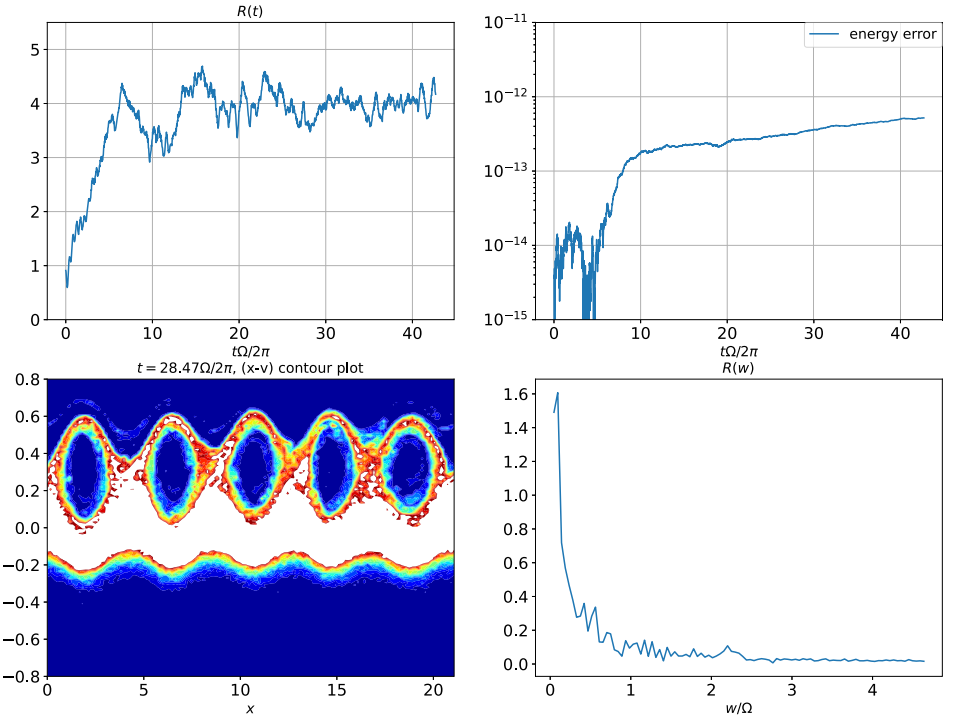

FIGURE 6. Simulations with the ponderomotive driving term by discrete gradient method. Time evolutions of $R(t) = \max(\phi/\tilde{\phi}_0)$ and energy error, the contour plot of the distribution function at time $t = 400$, and the fast Fourier transformation of $R(t)$.

simulation parameters used in § 6.3. The author would like to acknowledge P.J. Morrison, S. Possanner and E. Sonnendrücker for their kind discussions of this work.

Editor L.O. Silva thanks the referees for their advice in evaluating this article.

Declaration of interests

The author reports no conflict of interest.

Appendix A. Discretization with finite element method

Distribution function f is approximated using δ functions, i.e.

$$f(x, v, t) \approx f_h(x, v, t) = \sum_{k=1}^{N_p} w_k \delta(x - x_k)\delta(v - v_k), \tag{A1}$$

where N_p is the total particle number, and w_k, x_k, and v_k are the weight, position and velocity for the kth particle. We discretize ϕ by the finite element method, i.e.

$$\phi_h = \boldsymbol{\Lambda} \cdot \boldsymbol{\phi}, \tag{A2}$$

https://doi.org/10.1017/S0022377824001053 Published online by Cambridge University Press

where the vectors $\boldsymbol{\Lambda}$ and $\boldsymbol{\phi}$ contain all basis functions and finite element coefficients. The Poisson–Boltzmann equation is discretized in a weak formulation as

$$\int \partial_x \phi_h \partial_x \Lambda_i \,\mathrm{d}x + \underbrace{\int n_0 \exp\left(\frac{\phi_h - \phi_{0,h}}{T_e}\right) \Lambda_i \,\mathrm{d}x}_{\approx \sum_{j=1}^{N} w_j n_0(x_j) \exp\left(\frac{\phi_h(x_j) - \phi_{0,h}(x_j)}{T_e(x_j)}\right) \Lambda_i(x_j)} = Z \sum_{k=1}^{N_p} w_k \Lambda_i(x_k), \tag{A3}$$

where x_j is the jth quadrature point, and w_j is the corresponding quadrature weight. We define a matrix $\mathbf{M}$, with $\mathsf{M}_{ij} = \int \partial_x \Lambda_i \partial_x \Lambda_j \,\mathrm{d}x$.

We approximate variational action integral (2.6) as

$$\mathcal{A}_h = \sum_{k=1}^{N_p} w_k \left(\frac{\dot{x}_k^2}{2} - Z\phi_n(x_k)\right) + \boldsymbol{\phi}^\top \mathbf{M} \boldsymbol{\phi} + \sum_{j=1}^{N} w_j n_0(x_j) T_e(x_j) \exp\left(\frac{\phi_h(x_j) - \phi_{0,h}(x_j)}{T_e(x_j)}\right). \tag{A4}$$

Hamiltonian is discretized as

$$H = \sum_{k=1}^{N_p} w_k \frac{v_k^2}{2} + Z w_k \boldsymbol{\Lambda}(x_k) \cdot \boldsymbol{\phi} - \sum_{j=1}^{N} w_j T_e(x_j) n_0(x_j) \exp\left(\frac{\phi_h(x_j) - \phi_{0,h}(x_j)}{T_e(x_j)}\right) - \frac{\boldsymbol{\phi}^\top \mathbf{M} \boldsymbol{\phi}}{2}. \tag{A5}$$

As done by Qin *et al.* (2015*b*) and Kraus *et al.* (2017), the bracket is discretized as

$$\{F, G\}_h = \sum_{k=1}^{N_p} \frac{1}{w_k} \left(\partial_{x_k} F \partial_{v_k} G - \partial_{x_k} G \partial_{v_k} F\right). \tag{A6}$$

Both the variations of (A4) and the discrete Poisson bracket (A6) with Hamiltonian (A6) give the following Hamiltonian ordinary differential equation:

$$\dot{x}_k = \frac{1}{w_k} \partial_{v_k} H, \quad \dot{v}_k = -\frac{1}{w_k} \partial_{x_k} H. \tag{A7a,b}$$

Similarly, for the cases with periodic boundary conditions, we can prove that the neutrality condition holds in a weak sense, i.e.

$$\sum_{j=1}^{N} w_j n_0(x_j) \exp\left(\frac{\phi_h(x_j) - \phi_{0,h}(x_j)}{T_e(x_j)}\right) \Lambda_i(x_j) = Z \sum_{k=1}^{N_p} w_k \Lambda_i(x_k), \quad \forall i = 1, \ldots, N. \tag{A8}$$

https://doi.org/10.1017/S0022377824001053 Published online by Cambridge University Press

Appendix B. Hamiltonian splitting method for the electromagnetic hybrid model (Vu 1996)

We take the isothermal electron case with the following energy for an example:

$$\begin{aligned}\mathcal{H} = &\frac{1}{2}\int |\boldsymbol{v}|^2 f \,\mathrm{d}\boldsymbol{v}\,\mathrm{d}\boldsymbol{x} + \frac{1}{4}\int |Z\boldsymbol{a}|^2 f \,\mathrm{d}\boldsymbol{v}\,\mathrm{d}\boldsymbol{x} + \frac{1}{4}\int |\nabla a_1|^2 + |\nabla a_2|^2 + |\nabla a_3|^2 \,\mathrm{d}\boldsymbol{x} \\ &- \frac{1}{4\epsilon}\int |\boldsymbol{a}|^2 \,\mathrm{d}\boldsymbol{x} - \int T_e n_0 \exp\left(\frac{\phi - \dfrac{m_i}{4m_e}\boldsymbol{a}\cdot\boldsymbol{a}^*}{T_e}\right)\mathrm{d}\boldsymbol{x} \\ &- \frac{1}{2}\int |\nabla\phi|^2 \,\mathrm{d}\boldsymbol{x} + \int Zf\phi \,\mathrm{d}\boldsymbol{x}\,\mathrm{d}\boldsymbol{v}. \end{aligned} \tag{B1}$$

We split the Hamiltonian into the following three parts and get the corresponding explicitly solvable subsystems,

$$\begin{aligned}\mathcal{H} = &\underbrace{\frac{1}{2}\int |\boldsymbol{v}|^2 f \,\mathrm{d}\boldsymbol{v}\,\mathrm{d}\boldsymbol{x} + \frac{1}{4}\int |\nabla a_1|^2 + |\nabla a_2|^2 + |\nabla a_3|^2 \,\mathrm{d}\boldsymbol{x}}_{H_1} \\ &+ \underbrace{\frac{1}{4}\int |Z\boldsymbol{a}|^2 f \,\mathrm{d}\boldsymbol{v}\,\mathrm{d}\boldsymbol{x} - \frac{1}{4\epsilon}\int |\boldsymbol{a}|^2 \,\mathrm{d}\boldsymbol{x}}_{H_2} \\ &\underbrace{- \int T_e n_0 \exp\left(\frac{\phi - \dfrac{m_i}{4m_e}\boldsymbol{a}\cdot\boldsymbol{a}^*}{T_e}\right)\mathrm{d}\boldsymbol{x} - \frac{1}{2}\int |\nabla\phi|^2 \,\mathrm{d}\boldsymbol{x} + \int Zf\phi \,\mathrm{d}\boldsymbol{x}\,\mathrm{d}\boldsymbol{v}}_{H_3}. \end{aligned} \tag{B2}$$

Subsystem H_1. The corresponding subsystem is

$$\frac{\partial f}{\partial t} + \boldsymbol{v}\cdot\frac{\partial f}{\partial \boldsymbol{x}} = 0, \quad \mathrm{i}\epsilon\frac{\partial \boldsymbol{a}}{\partial t} = -\frac{\epsilon^2}{2}\Delta\boldsymbol{a}, \tag{B3a,b}$$

where the first equation is an explicitly solvable transport equation and the second equation can be solved explicitly in Fourier space.

Subsystem H_2. The corresponding subsystem is

$$\frac{\partial f}{\partial t} - \frac{Z^2}{4}\nabla(\boldsymbol{a}\cdot\boldsymbol{a}^*)\cdot\frac{\partial f}{\partial \boldsymbol{v}} = 0, \quad \mathrm{i}\epsilon\frac{\partial \boldsymbol{a}}{\partial t} = -\frac{1}{2}\left(1 - \epsilon^2 Z^2\int f\,\mathrm{d}\boldsymbol{v}\right)\boldsymbol{a}, \tag{B4a,b}$$

where the $\boldsymbol{a}\cdot\boldsymbol{a}^*$ is preserved by the second equation and $\int f\,\mathrm{d}\boldsymbol{v}$ is preserved by the first equation, which make the two equations explicitly solvable.

Subsystem H_3. The corresponding subsystem is

$$\frac{\partial f}{\partial t} - Z\nabla\phi\cdot\frac{\partial f}{\partial \boldsymbol{v}} = 0, \quad \mathrm{i}\epsilon\frac{\partial \boldsymbol{a}}{\partial t} = \frac{1}{2}\epsilon^2 n_e\frac{m_i}{m_e}\boldsymbol{a}, \quad -\Delta\phi = Z\int f\,\mathrm{d}\boldsymbol{v} - n_e, \tag{B5a–c}$$

where $\boldsymbol{a}\cdot\boldsymbol{a}^*$ is preserved by the second equation and the ion density $\int f\,\mathrm{d}\boldsymbol{v}$ is preserved by the first equation. As n_e depends on ϕ and $\boldsymbol{a}\cdot\boldsymbol{a}^*$, and $\boldsymbol{a}\cdot\boldsymbol{a}^*$ and $\int f\,\mathrm{d}\boldsymbol{v}$ are not changed

https://doi.org/10.1017/S0022377824001053 Published online by Cambridge University Press

in this sub-system, ϕ and n_e are preserved by this subsystem. We only need to solve the third equation for obtaining ϕ once in each time step, and the first and second equations are explicitly solvable.

REFERENCES

BAO, W., JIN, S. & MARKOWICH, P.A. 2002 On time-splitting spectral approximations for the Schrödinger equation in the semiclassical regime. *J. Comput. Phys*. **175** (2), 487–524.

BARDOS, C., GOLSE, F., NGUYEN, T.T. & SENTIS, R. 2018 The Maxwell–Boltzmann approximation for ion kinetic modeling. *Physica* D **376**, 94–107.

BIRDSALL, C.K. & LANGDON, A.B. 2018 *Plasma Physics via Computer Simulation*. CRC Press.

BYCHENKOV, V.Y., NOVIKOV, V.N., BATANI, D., TIKHONCHUK, V.T. & BOCHKAREV, S.G. 2004 Ion acceleration in expanding multispecies plasmas. *Phys. Plasmas* **11** (6), 3242–3250.

CAMPOS PINTO, M., AMERES, J., KORMANN, K. & SONNENDRÜCKER, E. 2024 On variational Fourier particle methods. *J. Sci. Comput.* **101** (3), 68.

CARTWRIGHT, K.L., VERBONCOEUR, J.P. & BIRDSALL, C.K. 2000 Nonlinear hybrid Boltzmann–particle-in-cell acceleration algorithm. *Phys. Plasmas* **7** (8), 3252–3264.

CHEN, L., HOLST, M.J. & XU, J. 2007 The finite element approximation of the nonlinear Poisson–Boltzmann equation. *SIAM J. Numer. Anal*. **45** (6), 2298–2320.

CHENG, C.-Z. & KNORR, G. 1976 The integration of the Vlasov equation in configuration space. *J. Comput. Phys*. **22** (3), 330–351.

COHEN, B.I., LASINSKI, B.F., LANGDON, A.B. & WILLIAMS, E.A. 1997 Resonantly excited nonlinear ion waves. *Phys. Plasmas* **4** (4), 956–977.

CROUSEILLES, N., EINKEMMER, L. & FAOU, E. 2015 Hamiltonian splitting for the Vlasov–Maxwell equations. *J. Comput. Phys*. **283**, 224–240.

DEGOND, P., LIU, H., SAVELIEF, D. & VIGNAL, M.-H. 2012 Numerical approximation of the Euler–Poisson–Boltzmann model in the quasineutral limit. *J. Sci. Comput*. **51**, 59–86.

FENG, K. & QIN, M. 2010 *Symplectic Geometric Algorithms for Hamiltonian Systems*, vol. 449. Springer.

GONZALEZ, O. 1996 Time integration and discrete Hamiltonian systems. *J. Nonlinear Sci*. **6**, 449–467.

GU, A., HE, Y. & SUN, Y. 2022 Hamiltonian particle-in-cell methods for Vlasov–Poisson equations. *J. Comput. Phys*. **467**, 111472.

HAIRER, E., LUBICH, C. & WANNER, G. 2006 *Geometric Numerical Integration: Structure-Preserving Algorithms for Ordinary Differential Equations*, vol. 31. Springer Science & Business Media.

HE, Y., QIN, H., SUN, Y., XIAO, J., ZHANG, R. & LIU, J. 2015 Hamiltonian time integrators for Vlasov–Maxwell equations. *Phys. Plasmas* **22** (12), 124503.

HE, Y., SUN, Y., QIN, H. & LIU, J. 2016 Hamiltonian particle-in-cell methods for Vlasov–Maxwell equations. *Phys. Plasmas* **23** (9), 092108.

HEATH, R.E., GAMBA, I.M., MORRISON, P.J. & MICHLER, C. 2012 A discontinuous galerkin method for the Vlasov–Poisson system. *J. Comput. Phys*. **231** (4), 1140–1174.

HOCKNEY, R.W. & EASTWOOD, J.W. 2021 *Computer Simulation using Particles*. CRC Press.

HOLDERIED, F., POSSANNER, S. & WANG, X. 2021 MHD-kinetic hybrid code based on structure-preserving finite elements with particles-in-cell. *J. Comput. Phys*. **433**, 110143.

HU, Y. & WANG, J. 2018 Expansion of a collisionless hypersonic plasma plume into a vacuum. *Phys. Rev.* E **98** (2), 023204.

HUANG, C.-K., ZENG, Y., WANG, Y., MEYERS, M.D., YI, S. & ALBRIGHT, B.J. 2016 Finite grid instability and spectral fidelity of the electrostatic particle-in-cell algorithm. *Comput. Phys. Commun*. **207**, 123–135.

JIN, S. 1999 Efficient asymptotic-preserving (AP) schemes for some multiscale kinetic equations. *SIAM J. Sci. Comput*. **21** (2), 441–454.

KELLEY, C T. 1995. *Iterative methods for linear and nonlinear equations*. Society for Industrial and Applied Mathematics.

KORMANN, K. & SONNENDRÜCKER, E. 2021 Energy-conserving time propagation for a structure-preserving particle-in-cell Vlasov–Maxwell solver. *J. Comput. Phys*. **425**, 109890.

https://doi.org/10.1017/S0022377824001053 Published online by Cambridge University Press

Kraus, M., Kormann, K., Morrison, P.J. & Sonnendrücker, E. 2017 GEMPIC: geometric electromagnetic particle-in-cell methods. *J. Plasma Phys*. **83** (4), 905830401.

Kunz, M.W., Stone, J.M. & Bai, X.-N. 2014 Pegasus: a new hybrid-kinetic particle-in-cell code for astrophysical plasma dynamics. *J. Comput. Phys*. **259**, 154–174.

Li, Y., Campos-Pinto, M., Holderied, F., Possanner, S. & Sonnendrücker, E. 2024*a* Geometric particle-in-cell discretizations of a plasma hybrid model with kinetic ions and mass-less fluid electrons. *J. Comput. Phys*. **498**, 112671.

Li, Y., Holderied, F., Possanner, S. & Sonnendrücker, E. 2024*b* Canonical variables based numerical schemes for hybrid plasma models with kinetic ions and massless electrons. *J. Comput. Phys.* **505**, 112916.

Low, F.E. 1958 A lagrangian formulation of the Boltzmann–Vlasov equation for plasmas. *Proc. R. Soc. Lond.* A **248** (1253), 282–287.

Lu, B.Z., Zhou, Y.C., Holst, M.J. & McCammon, J.A. 2008 Recent progress in numerical methods for the Poisson–Boltzmann equation in biophysical applications. *Commun. Comput. Phys*. **3** (5), 973–1009.

Manzini, G., Delzanno, G.L., Vencels, J. & Markidis, S. 2016 A Legendre–Fourier spectral method with exact conservation laws for the Vlasov–Poisson system. *J. Comput. Phys*. **317**, 82–107.

Marsden, J.E. & Ratiu, T.S. 2013 *Introduction to Mechanics and Symmetry: A Basic Exposition of Classical Mechanical Systems*, vol. 17. Springer Science & Business Media.

McLachlan, R.I., Quispel, G.R.W. & Robidoux, N. 1999 Geometric integration using discrete gradients. *Phil. Trans. R. Soc. Lond.* A **357** (1754), 1021–1045.

Morrison, P.J. 1980 The Maxwell–Vlasov equations as a continuous Hamiltonian system. *Phys. Lett.* A **80** (5–6), 383–386.

Morrison, P.J. 2017 Structure and structure-preserving algorithms for plasma physics. *Phys. Plasmas* **24** (5), 055502.

Qin, H., He, Y., Zhang, R., Liu, J., Xiao, J. & Wang, Y. 2015*a* Comment on "Hamiltonian splitting for the Vlasov–Maxwell equations". *J. Comput. Phys*. **297**, 721–723.

Qin, H., Liu, J., Xiao, J., Zhang, R., He, Y., Wang, Y., Sun, Y., Burby, J.W., Ellison, L. & Zhou, Y. 2015*b* Canonical symplectic particle-in-cell method for long-term large-scale simulations of the Vlasov–Maxwell equations. *Nucl. Fusion* **56** (1), 014001.

Rambo, P.W. 1995 Finite-grid instability in quasineutral hybrid simulations. *J. Comput. Phys*. **118** (1), 152–158.

Rambo, P.W. 1997 Numerical heating in hybrid plasma simulations. *J. Comput. Phys*. **133** (1), 173–180.

Sonnendrücker, E. 2017 *Numerical Methods for the Vlasov–Maxwell Equations*. Springer.

Sonnendrücker, E., Roche, J., Bertrand, P. & Ghizzo, A. 1999 The semi-lagrangian method for the numerical resolution of the Vlasov equation. *J. Comput. Phys*. **149** (2), 201–220.

Stanier, A., Chacón, L. & Chen, G. 2019 A fully implicit, conservative, non-linear, electromagnetic hybrid particle-ion/fluid-electron algorithm. *J. Comput. Phys*. **376**, 597–616.

Tajima, T. 2018 *Computational Plasma Physics: With Applications to Fusion and Astrophysics*. CRC Press.

Vu, H.X. 1996 An adiabatic fluid electron particle-in-cell code for simulating ion-driven parametric instabilities. *J. Comput. Phys*. **124** (2), 417–430.

Vu, H.X., Bezzerides, B. & DuBois, D.F. 1999 ASPEN: a fully kinetic, reduced-description particle-in-cell model for simulating parametric instabilities. *J. Comput. Phys*. **156** (1), 12–42.

Webb, S.D. 2016 A spectral canonical electrostatic algorithm. *Plasma Phys. Control. Fusion* **58** (3), 034007.

Xiao, J. & Qin, H. 2019*a* Field theory and a structure-preserving geometric particle-in-cell algorithm for drift wave instability and turbulence. *Nucl. Fusion* **59** (10), 106044.

Xiao, J. & Qin, H. 2019*b* Structure-preserving geometric particle-in-cell algorithm suppresses finite-grid instability–comment on 'finite grid instability and spectral fidelity of the electrostatic Particle-In-Cell algorithm' by huang *et al.* arXiv:1904.00535.

Xiao, J., Qin, H., Liu, J., He, Y., Zhang, R. & Sun, Y. 2015 Explicit high-order non-canonical symplectic particle-in-cell algorithms for Vlasov–Maxwell systems. *Phys. Plasmas* **22** (11), 112504.

XU, Z. & CAI, W. 2011 Fast analytical methods for macroscopic electrostatic models in biomolecular simulations. *SIAM Rev*. **53** (4), 683–720.

YIN, P., HUANG, Y. & LIU, H. 2014 An iterative discontinuous galerkin method for solving the nonlinear Poisson–Boltzmann equation. *Commun. Comput. Phys*. **16** (2), 491–515.

YIN, P., HUANG, Y. & LIU, H. 2018 Error estimates for the iterative discontinuous Galerkin method to the nonlinear Poisson–Boltzmann equation. *Commun. Comput. Phys*. **23** (1), 168–197.

ZHOU, Z., HE, Y., SUN, Y., LIU, J. & QIN, H. 2017 Explicit symplectic methods for solving charged particle trajectories. *Phys. Plasmas* **24** (5), 052507.

https://doi.org/10.1017/S0022377824001053 Published online by Cambridge University Press